diffusion-fundamentals

The Open-Access Journal for the Basic Principles of Diffusion Theory, Experiment and Application

Oxygen and Cation Diffusion Processes in Oxygen Ion Conductors

Manfred Martin
Institute of Physical Chemistry, RWTH Aachen University
Landoltweg 2, 52056 Aachen, Germany,
E-Mail: martin@rwth-aachen.de

Dedicated to Professor Hermann Schmalzried on the occasion of his 75th birthday.

Abstract

We discuss oxygen and cation diffusion processes in oxygen ion conductors. While the high oxygen diffusivity determines the proper oxygen ion conductivity, slow cation diffusion processes are important for sintering and degradation processes. In the first part of the paper we discuss an analytical model for the ionic conductivity of a strongly acceptor doped, fluorite-type oxygen ion conductor, i.e. a concentrated solution of AO_2 and B_2O_3. The model can be applied, e.g., to yttria doped zirconia (YSZ) and gives a qualitative explanation of the observed maximum of the conductivity as a function of the dopant fraction. The model considers nearest neighbor interactions between oxygen vacancies and dopant cations, which may be negligible, attractive or repulsive, and jump barriers that depend on the nature of the cation-cation edge that has to be crossed during a jump between adjacent oxygen sites. In the second part we discuss cation diffusion processes in doped lanthanum gallates (LSGM). The experimental results of nearly identical cation diffusion coefficients in the A- and B-sublattices of the perovskite LSGM can be explained by a bound defect cluster mechanism containing cation vacancies of both the A- and the B- sublattice and anion vacancies.

Keywords: diffusion, defects, oxygen diffusion, oxygen ion conductivity, cation diffusion, cluster mechanism

1. Introduction

Diffusion processes in crystalline oxides are largely determined by point defects and their mobilities. For the understanding of the defect structure of oxides we must consider the following points:

- Most oxides are ionic compounds, i.e. they consist of cations and anions with well defined, opposite charges.
- Crystalline oxides consist of at least two sublattices, a metal and an oxygen sublattice, or a cation and an anion sublattice. Due to the opposite charges of cations and anions diffusion proceeds always in the corresponding sublattice.
- The concentrations of point defects, vacancies as well as interstitials, which are necessary for diffusion depend not only on the intensive thermodynamic variables pressure, p, and temperature, T, but also on the partial pressure pO_2 of the component oxygen. The latter can be established easily by means of gas mixtures and can be varied over many orders of magnitude.

- Oxides cover a wide range of materials, such as insulators, pure ionic conductors, semiconductors, mixed electronic and ionic conductors and also metallic oxides.
- The crystal structure of the oxide influences the defect structure. In structures with cubic close packing of the oxygen ions, such as the NaCl- or the spinel-structure, defects in the oxygen sublattice have much higher formation enthalpies and therefore much lower concentrations than defects in the cation sublattice(s). Consequently, oxygen diffusion is much slower than cation diffusion. In oxides with more open oxygen sublattices, such as the perovskite structure or the fluorite structure, oxygen defects are formed more easily than cation defects. Therefore, these oxides show very often high oxygen diffusivities and are good oxygen ion conductors.

These introductory remarks show that diffusion in oxides depends largely on the defect structure of the oxide. The important dependence of the defect structure on the thermodynamic variables p, T and pO_2 (so-called defect chemistry) and a comprehensive treatment of diffusion processes can be found, e.g., in the books of Schmalzried [1] and Allnatt and Lidiard [2].

In this article we will focus on diffusion processes in oxides with dominating oxygen disorder. A detailed treatment of oxides with dominating cation disorder can be found in [3]. Important examples for dominating oxygen disorder are oxides crystallizing in the fluorite or the perovskite structure. To increase the fraction of oxygen vacancies, the oxide, e.g. AO_2, is doped with oxides of lower valent metals. Then, charge neutrality requires $[B'_A] = 2[V_O^{\bullet\bullet}]$, i.e. the negative excess charge of the acceptor dopant, B'_A, is compensated by oxygen vacancies, $V_O^{\bullet\bullet}$, and the doped oxide may become a good oxygen ion conductor. Two well know examples are:

- Yttria-stabilized zirconia, $(Zr_{1-x}Y_x)O_{2-x/2}$ (YSZ). Here, doping with Y_2O_3 increases the fraction of oxygen vacancies, $[Y'_{Zr}] = 2[V_O^{\bullet\bullet}]$, and stabilizes the cubic fluorite structure. YSZ is a pure oxygen ion conductor over many orders of magnitude in pO_2 and is used as such in oxygen sensors and solid oxygen fuel cells (SOFC) (see e.g. [4] and references therein).

- Sr- and Mg-doped lanthanum gallate, $(La_{1-x}Sr_x)(Ga_{1-y}Mg_y)O_{3-(x+y)/2}$ (LSGM), which belongs to the class of perovskites ABO_3. In LSGM oxygen vacancies are produced by co-doping in both cation sublattices, $[Sr'_{La}] + [Mg'_{Ga}] = 2[V_O^{\bullet\bullet}]$, resulting also in a good oxygen ion conductor (see e.g. [4] and references therein).

Subsequently, we will first discuss the oxygen ion conductivity in YSZ, i.e. we will consider the highly concentrated, mobile majority defects (oxygen vacancies). In the second part we will discuss cation diffusion in LSGM, i.e. here we will consider the highly diluted, mobile minority defects (cation vacancies).

2. Oxygen ion conductivity in fluorite-type oxygen ion conductors

Acceptor-doped, stabilized zirconia, e.g. yttria-doped zirconia (YSZ), exhibits high oxygen ion conductivity and has therefore many applications, e.g. in fuel cells, oxygen sensors, etc. (for an overview see [5]). YSZ and zirconia doped with other dopants, B, have been studied extensively for many years by measuring the oxygen ion conductivities and the tracer diffusion coefficients of oxygen as a function of the dopant concentration and the temperature (see [5,6,7] and references therein). While it is well accepted that the majority point defects are oxygen vacancies and acceptor dopants, there is still discussion on the origin of the maximum in the ionic conductivity as a function of the dopant fraction which is observed at dopant levels $x_B \approx 0.15$ (x_B is the B-fraction in the cation sublattice) [8,9]. One of the first attempts to explain these findings goes back to Schmalzried [10] who showed that ordering of the vacancies and correlation effects cause a decrease of the conductivity with increasing dopant fraction. In other investigations the maximum was attributed to the interaction between dopants and oxygen vacancies, which is expected to be attractive, due to the opposite charges of both defects. Thus, in a simple picture, oxygen vacancies are trapped by the immobile dopant ions and do not contribute in the same way to the conductivity as free vacancies. However, atomistic simulations have shown that lattice relaxation near the dopant plays an important role and that the interaction energy between dopant cations and vacancies depends on the ionic radius of the dopant and the position of the vacancy [11,12]. Dopants with smaller ionic radii than Zr (undersized dopants) prefer nearest neighbor positions, while dopants with larger ionic radii (oversized dopants, e.g. Y) prefer next-nearest neighbor positions. However, these calculations were performed for infinitely diluted dopants, and it is doubtful that the results can be applied to solid solutions where the dopant fraction is as high as $x_B \approx 0.15$. Another origin of the maximum in the ionic conductivity was suggested by Shimojo et al. [13,14] using molecular dynamics (MD). In the fluorite structure, oxygen ions occupy tetrahedra formed by the cations. During a jump between two adjacent tetrahedra, the oxygen ion has to cross the common edge of the two tetrahedra. According to the MD-studies, the jump rate through an Y-Y edge is drastically reduced compared to the jump rate through a Zr-Zr edge (probably caused by size effects). With increasing dopant fraction the number of Y-Y edges increases and, thus, the oxygen ion conductivity decreases. Monte Carlo studies have been performed by Meyer and Nicoloso [15] considering three models. In the first model they assumed only attractive interactions between dopant ions and vacancies, in the second model only repulsive interactions, and the third model was a barrier model as suggested by Shimojo [13,14]. Only the barrier model was able to reproduce the experimentally obtained maximum in the conductivity. Murray at al. [16] have performed detailed Monte Carlo studies after having calculated the jump activation energies with atomistic simulation methods and could explain the maximum qualitatively. Recently, Krishnamurthy et al. [17] used density functional theory methods to calculate the migration energies for vacancy jumps through different edges and confirmed that the activation energies for jumps through Zr-Y and Y-Y edges, 1.29 eV and 1.86 eV, are much higher than the value for a jump across a Zr-Zr edge, 0.58 eV. However, in the subsequent Monte Carlo analysis the authors calculated the oxygen ion conductivity assuming only a random vacancy distribution.

Here we discuss a simple analytical model for the oxygen ion conductivity of fluorite-type oxygen ion conductors [18,19] which can be used for a concentrated solution of host cations A and dopant cations B, and explains the important experimental findings for YSZ:

- maximum of conductivity at dopant fractions $x_B \approx 0.15$ [8,9]
- slight decrease of the activation energy with increasing temperature [20]
- increase of the activation energy with increasing dopant fraction [21].

In section 2.1 the distribution function for different cation tetrahedra in the fluorite structure is discussed considering for simplicity a statistical distribution of host cations A and dopant cations B. Then, the distribution of oxygen vacancies to the different oxygen sites is analyzed using quasi-chemical reactions and considering dopant-vacancy interaction. We restrict the interactions to nearest neighbor interactions, i.e. vacancies interact only with nearest neighbor B-cations (maximum 4). In section 2.2 a model for the ionic conductivity, σ, is introduced, and the dependence of σ on the dopant fraction is calculated using the results for the oxygen vacancy distribution of section 2.1.

2.1 Vacancy distribution

In the fluorite structure the N cations form a fcc lattice where each cation has 6 nearest neighbor cations. The oxygen ions occupy the 2N tetrahedral interstices thereby forming a cubic lattice where each anion has 6 nearest neighbor anion sites. A fraction x_A of the N cation sites is occupied by host cations, A ($\equiv A_A^x$), while a fraction $x_B = 1 - x_A$ is occupied by trivalent dopant ions, B ($\equiv B_A'$). Their negative excess charge is compensated by oxygen vacancies, V ($\equiv V_O^{\bullet\bullet}$), with $x_B=2x_V$, corresponding to $(A_{1-x_B}B_{x_B})O_{2-x_B/2}$. Cation vacancies are only minority defects and are neglected. In our model, we want to treat a "concentrated" solution of host cations, A, and dopant cations, B. For simplicity, we consider a statistical cation distribution (cation clustering was treated in [18]). Then, the fractions $f_n(x_B)$ of tetrahedra consisting of n B-cations (n = 0,1,2,3,4) are given by (see also [15])

$$f_n(x_B) = 2\binom{4}{n} x_B^n (1-x_B)^{4-n} \qquad (1)$$

The sum of all fractions is equal to 2, which is the number of tetrahedra per cation. The individual fractions are shown in Fig. 1. Subsequently we will use the following notation for the fractions of tetrahedra, [ijkl] with (i,j,k,l = A,B), where [AAAA] = f_0, [AAAB] = f_1 etc.

Knowing the cation distribution (or the tetrahedra distribution), we have to distribute the oxygen vacancies on the oxygen sublattice. Oxygen ions, O ($\equiv O_O^x$), and oxygen vacancies, V, occupy the 2N tetrahedra formed by the N cations. Since we have assumed only nearest neighbor interactions between oxygen vacancies, V, and dopant cations, B, oxygen ions and oxygen vacancies can exist with five different tetrahedral cation surroundings, AAAA, AAAB, AABB, ABBB and BBBB.

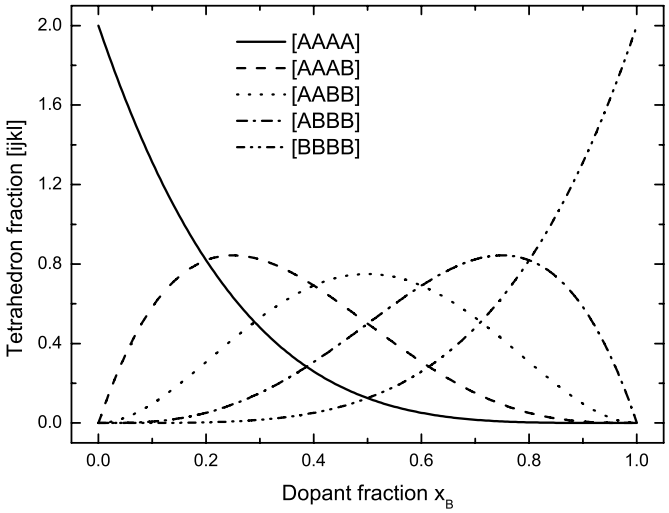

Fig. 1 Fractions of tetrahedra AAAA, AAAB, AABB, ABBB, and BBBB according to Eq.(1).

The equilibrium between oxygen vacancies in the five different tetrahedra is described by four quasi-chemical reactions

$$V_{AAAA} + O_{AAAB} \longleftrightarrow O_{AAAA} + V_{AAAB} \qquad K_1 = \frac{[O_{AAAA}]\cdot[V_{AAAB}]}{[V_{AAAA}]\cdot[O_{AAAB}]} \quad K_1 = \exp\left(-\frac{\Delta E_1}{kT}\right) \tag{2}$$

$$V_{AAAA} + O_{AABB} \longleftrightarrow O_{AAAA} + V_{AABB} \qquad K_2 = \frac{[O_{AAAA}]\cdot[V_{AABB}]}{[V_{AAAA}]\cdot[O_{AABB}]} \quad K_2 = \exp\left(-\frac{\Delta E_2}{kT}\right) \tag{3}$$

$$V_{AAAA} + O_{ABBB} \longleftrightarrow O_{AAAA} + V_{ABBB} \qquad K_3 = \frac{[O_{AAAA}]\cdot[V_{ABBB}]}{[V_{AAAA}]\cdot[O_{ABBB}]} \quad K_3 = \exp\left(-\frac{\Delta E_3}{kT}\right) \tag{4}$$

$$V_{AAAA} + O_{BBBB} \longleftrightarrow O_{AAAA} + V_{BBBB} \qquad K_3 = \frac{[O_{AAAA}]\cdot[V_{BBBB}]}{[V_{AAAA}]\cdot[O_{BBBB}]} \quad K_4 = \exp\left(-\frac{\Delta E_4}{kT}\right) \tag{5}$$

Here ΔE_n (n = 1,2,3,4) is the "binding energy" of a vacancy inside a tetrahedron consisting of n B-cations. It is given by the energy difference between a vacancy in that tetrahedron and a vacancy in an AAAA-tetrahedron. Entropic contributions to the mass action constants K_i are believed to be negligible. $[V_{ijkl}]$ and $[O_{ijkl}]$ (i,j,k,l = A,B) are the fractions of oxygen vacancies and oxygen ions sitting inside ijkl-tetrahedra. In addition, we have to consider the condition of charge neutrality, $x_B = 2x_V$.

$$x_B = 2\left([V_{AAAA}] + [V_{AAAB}] + [V_{AABB}] + [V_{ABBB}] + [V_{BBBB}]\right) \tag{6}$$

From Eqs. (1)-(6) the fractions of vacancies occupying ijkl-tetrahedra, $[V_{ijkl}]$, can be calculated as a function of the dopant fraction, x_B, and the temperature T (using the results for the cation distribution in Eq. (1)).

Fig. 2 shows the vacancy fractions for vanishing interaction between B-cations and oxygen vacancies (statistical vacancy distribution) and for attractive interaction. For simplicity we have assumed that the total B-V interaction energy in a tetrahedron containing n B-cations is given by $\Delta E_n = n \cdot \Delta E_1$ (n = 0,1,2,3,4).

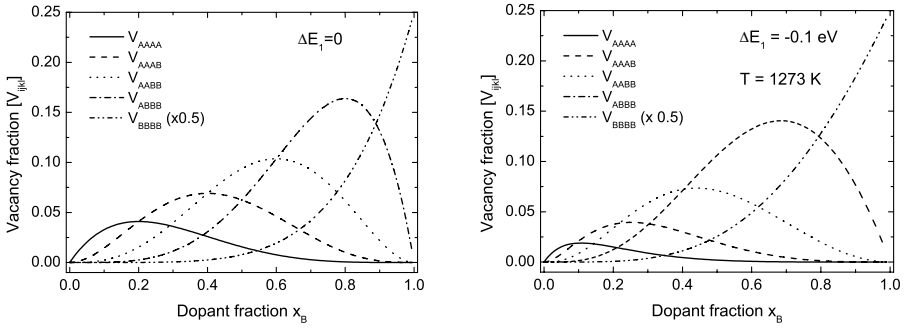

Fig. 2 Oxygen vacancy fractions, $[V_{ijkl}]$ (i,j,k,l=A,B), in different tetrahedra as a function of the dopant fraction, x_B, at T = 1273 K. (a) vanishing dopant-vacancy interaction energy, ΔE_1 = 0 (b) attractive dopant-vacancy interaction, ΔE_1 = -0.1 eV.

The binding energy, ΔE_1 = -0.1 eV, that was used in Fig. 2b is typical for dopant ions in YSZ [11,12]. Compared to the statistical vacancy distribution the probability to find a vacancy inside tetrahedra containing B-cations has increased. For repulsive interaction between dopants and vacancies (not shown in Fig.2) the fraction of vacancies occupying B-tetrahedra decreases [19].

2.2 Oxygen ion conductivity

Simple conductivity models where all vacancies contribute to the conductivity in the same way, i.e. with the same mobility, $\sigma = \text{const} \cdot [V] = \text{const} \cdot (x_B / 2)$, and models considering site blocking $\sigma = \text{const} \cdot [V] \cdot (1 - [V]) = \text{const} \cdot (x_B / 2) \cdot (1 - x_B / 2)$ cannot explain the experimentally observed maximum in the conductivity nor the dependence of the conductivity on the chemical nature of the dopant. Thus, we must consider the microscopic jump processes of vacancies and their jump rates, ω, in more detail. Since we have restricted the B-V interactions to nearest neighbor interactions, the vacancy jump rate from one specific site to an adjacent specific site depends only on the nearest neighbor cation configuration of the vacancy before the jump (i.e. the type of tetrahedron) and the nature of the edge which has to be crossed (A-A, A-B or B-B). The resulting 9 jump frequencies are denoted by $\omega_{n,m}$ where n and m are the numbers of B-cations in the tetrahedron before

the jump and in the edge to be crossed (see Fig. 3). Due to detailed balance, always two jump frequencies are coupled, e.g. $\omega_{1,0}/\omega_{0,0} = \exp(\Delta E_{10}/kT)$, where ΔE_{10} is the difference between the vacancy binding energies in the tetrahedra AAAB (ΔE_1) and AAAA (ΔE_0). In summary, there are only three independent frequencies, which can be taken as $\omega_{0,0}$, $\omega_{1,1}$ and $\omega_{2,2}$ (for details see [19]).

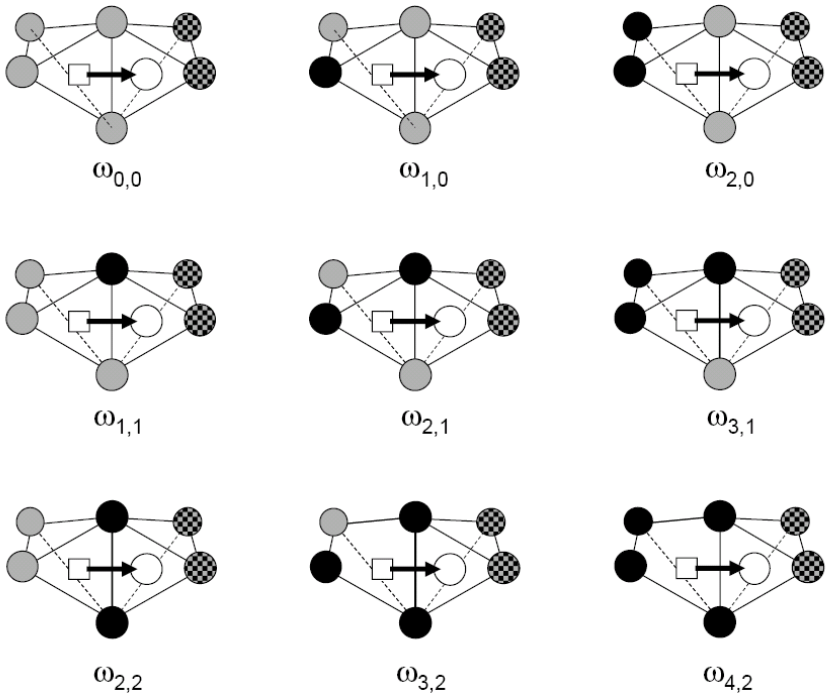

Fig. 3 Jump rates of oxygen vacancies, $\omega_{n,m}$, from a tetrahedron with n B-cations through an edge with m B-cations (grey circle = A, black circle = B, grey/black circle = A or B).

An oxygen vacancy inside an AAAA-tetrahedron can perform 6 jumps through the six edges with a jump frequency $\omega_{0,0}$. A neighboring tetrahedron must be of the type AAAA, AAAB or AABB (sharing an A-A edge with the AAAA-tetrahedron) and it must not be occupied by a vacancy. Thus, the probability for the neighboring tetrahedron to be accessible is $[O_{AAAA}]+[O_{AAAB}]+[O_{AABB}]$ and the partial ionic conductivity of vacancies V_{AAAA} is given by $\sigma(V_{AAAA}) = \text{const}\cdot[V_{AAAA}]\cdot 6\cdot\omega_{0,0}\cdot\left([O_{AAAA}]+[O_{AAAB}]+[O_{AABB}]\right)$.

Counting the contributions of the other vacancies in a similar way, we obtain finally:

$$\sigma = \text{const}\cdot\Big([V_{AAAA}]\cdot 6\cdot\omega_{0,0}\cdot([O_{AAAA}]+[O_{AAAB}]+[O_{AABB}])$$
$$+[V_{AAAB}]\cdot\{3\cdot\omega_{1,0}\cdot([O_{AAAA}]+[O_{AAAB}]+[O_{AABB}])+3\cdot\omega_{1,1}\cdot([O_{AAAB}]+[O_{AABB}]+[O_{ABBB}])\}$$
$$+[V_{AABB}]\cdot\begin{Bmatrix}+\omega_{2,0}\cdot([O_{AAAA}]+[O_{AAAB}]+[O_{AABB}])+\omega_{2,2}\cdot([O_{AABB}]+[O_{ABBB}]+[O_{BBBB}])\\+4\omega_{2,1}\cdot([O_{AAAB}]+[O_{AABB}]+[O_{ABBB}])\end{Bmatrix}$$
$$+[V_{ABBB}]\cdot\{3\cdot\omega_{3,2}\cdot([O_{AABB}]+[O_{ABBB}]+[O_{BBBB}])+3\cdot\omega_{3,1}\cdot([O_{AAAB}]+[O_{AABB}]+[O_{ABBB}])\}$$
$$+[V_{BBBB}]\cdot 6\cdot\omega_{4,2}\cdot([O_{AABB}]+[O_{ABBB}]+[O_{BBBB}])\Big) \quad (8)$$

To proceed we must specify all jump frequencies in terms of the dopant-vacancy interaction energy, ΔE_1, and the barrier energies, $\Delta E_{AA,}$ $\Delta E_{AB,}$ and ΔE_{BB}, for jumps across A-A, A-B and B-B edges. We will again consider the three cases, (I) statistical vacancy distribution, (II) attractive B-V interaction, and (III) repulsive B-V interaction. In addition, we will consider for each of the three cases (a) identical barrier energies (ΔE_{AA} = ΔE_{AB} = ΔE_{BB} = 0.58 eV), and (b) blocking A-B and B-B edges (ΔE_{AA} = 0.58 eV, ΔE_{AB} = 1.29 eV and ΔE_{BB} = 1.86 eV [17]). For T = 1273 K the results are shown in Fig. 4.

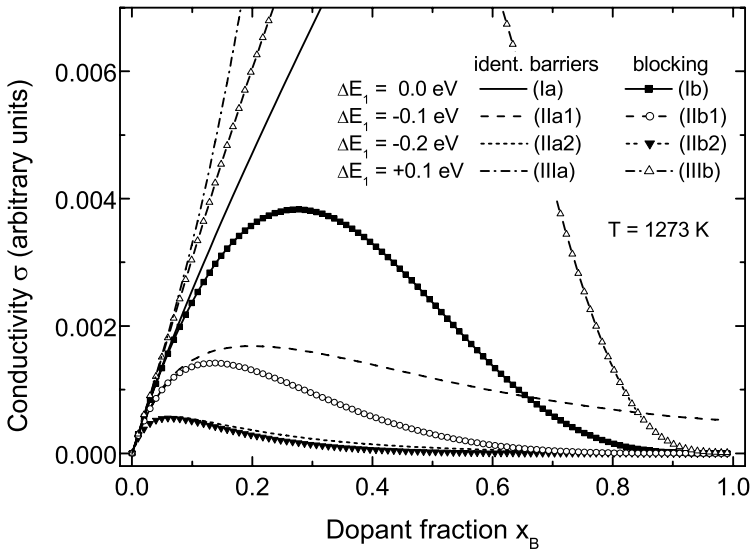

Fig. 4 Dependence of the oxygen ion conductivity, σ, on the dopant fraction, x_B, according to Eq. (8) at T = 1273 K (ΔE_1 = dopant-vacancy interaction energy; identical barriers: ΔE_{AA} = ΔE_{AB} = ΔE_{BB} = 0.58 eV; blocking: ΔE_{AA} = 0.58 eV, ΔE_{AB} = 1.23 eV, ΔE_{BB} = 1.86 eV [17]).

Fig. 4 shows that for a statistical vacancy distribution and identical barrier energies the conductivity increases monotonically with the dopant fraction (in Fig. 4 only the initial part of the curve is shown) while for blocking A-B and B-B edges the conductivity goes through a maximum at $x_B \approx 0.27$. For weak dopant vacancy-binding, $\Delta E_1 = -0.1$ eV, and identical barriers the conductivity first increases with the same slope as before, goes then through a broad maximum at $x_B \approx 0.2$ and eventually decreases slowly. The maximum conductivity is about a factor 2 smaller than without binding. For stronger dopant vacancy-binding, $\Delta E_1 = -0.2$ eV, the maximum appears already at $x_B \approx 0.07$ and the maximum conductivity is about a factor 6 smaller than without binding. For blocking A-B and B-B edges the maximum appears already at $x_B \approx 0.13$ ($\Delta E_1 = -0.1$ eV) and the conductivity maximum is sharper than without edge blocking. The maximum conductivity is only slightly smaller than without blocking. For stronger dopant vacancy-binding, $\Delta E_1 = -0.2$ eV, edge blocking has only very slight influence on the conductivity curve. For repulsive B-V interaction, a maximum in the conductivity is only obtained with blocking A-B and B-B edges. In contrast to the other cases the maximum is very broad and close to $x_B = 0.5$.

As shown in [19], our model yields an activation energy, E_a, of the conductivity which decreases with increasing temperature, as observed experimentally [20], only for attractive B-V interaction. In all other cases, i.e. for vanishing or repulsive interaction, E_a remains essentially constant. Our model also predicts a dependence of the conductivity activation energy on the dopant fraction: A statistical vacancy distribution and identical barrier energies result in a constant activation energy, $E_a = 0.58$ eV, as expected. If we introduce blocking A-B and B-B edges the activation energy remains unchanged up to dopant fractions $x_B \approx 0.6$, i.e. the vacancy follows essentially only jump pathways across A-A edges. Only for higher dopant fractions jump pathways across the blocking A-B and B-B edges start to contribute to the conductivity, and, consequently, the conductivity activation energy increases. For attractive dopant-vacancy interaction the conductivity activation energy increases monotonically with increasing dopant fraction, x_B, already for very small x_B. This behavior is due to the fact that already for small x_B more vacancies are trapped inside AAAB-tetrahedra than in AAAA-tetrahedra (see Fig. 2). With increasing dopant fraction more and more vacancies are trapped in tetrahedra containing n = 1,2, 3 or 4 B-cations. As a consequence the activation energy increases from 0.58 eV at $x_B = 0$ (n = 0) continuously to (0.58 + 4·0.1) eV = 0.98 eV at $x_B \approx 1$. If we introduce in addition blocking A-B and B-B edges the activation energy strongly increases for $x_B > 0.7$ showing that now also jumps across A-B edges start to contribute to the conductivity. For repulsive B-V interaction (case (III)) the activation energy slowly decreases with increasing dopant fraction from 0.58 eV (n = 0) to about (0.58 - 4·0.1) eV = 0.18 eV (n = 4).

2.3 Conclusions

We have presented a simple analytical model for a strongly acceptor doped fluorite-type oxygen ion conductor, i.e. a concentrated solution of AO_2 and B_2O_3. The model considers a statistical distribution of cations and interactions between oxygen vacancies and dopant cations. The oxygen vacancies were distributed to the AAAA-, AAAB-, AABB-, ABBB and BBBB-tetrahedra in the fluorite structure using quasi-chemical reac-

tions for the equilibrium between the different sites. The resulting vacancy distribution was then used in a simplified model for the ionic conductivity which considers different jump rates of oxygen vacancies that depend on the local configuration and the nature of the cation-cation edge that has to be crossed during a jump.

We have considered three cases for the vacancy distribution, (I) vanishing B-V interaction, (II) attractive B-V interaction, and (III) repulsive B-V interaction, and two cases for the jump activation energies through cation-cation edges, (a) identical jump energies and (b) blocking A-B and B-B edges. For case (Ia) (vanishing B-V interaction and identical barrier energies) and for case (IIIa) (repulsive B-V interaction and identical barrier energies) the conductivity increases monotonically with the dopant fraction. In all other cases we have found a maximum in the conductivity as a function of the dopant fraction. With increasing dopant fraction, the activation energy of the ionic conductivity remains constant in case (I), it increases in case (II), and it deceases in case (III) (for $x_B < 0.7$).

If we consider the experimental findings in YSZ (narrow conductivity maximum at $x_B \approx 0.15$, conductivity activation energy that decreases with increasing x_B and slightly decreases with increasing temperature [8,9,20,21]) we can conclude that only weak attractive interaction between Y and oxygen vacancies combined with blocking Y-Zr and Y-Y edges can reproduce the experimental data.

Another experimental finding concerns the dependence of the conductivity on the type of dopant. Badwal et al. [20] investigated the conductivity of zirconia that is co-doped with Y and Sc. In a composition series from YSZ to ScSZ they found at $T >$ 1000K a continuous increase of the oxygen ion conductivity. According to atomistic simulations Sc has a smaller binding energy to vacancies than Y [11,12]. In addition, we expect the edge blocking effect of Sc to be smaller than that of Y because Sc has a smaller ionic radius than Y. Following our model, both effects result in an higher ionic conductivity of ScSZ compared to YSZ. Qualitatively ScSZ corresponds to case IIb1 in Fig. 4 and YSZ to case IIb2. Due to the smaller edge blocking effect our model predicts a broader conductivity maximum in ScSZ than in YSZ. However, to the author's knowledge experimental data for the dependence of the oxygen ion conductivity of ScSZ on the Sc-fraction are not available.

It must be emphasized that our model contains several approximations. We have limited all interactions to nearest neighbor interactions. Qualitatively, this might be justified due to the high ionic strength in these electrolytes and the resulting short Debye length. A more detailed analysis must consider also next-nearest neighbor interactions and possible binding at these sites as suggested in [11, 12]. Furthermore, we have neglected vacancy-vacancy interactions, which would influence the vacancy distribution and the vacancy jump rates. Correlation effects which are caused by the locally different jump rates were only considered in a first approximation and only for successive jumps (see Eq. (8)). In a more accurate analysis the correlation effects must be considered through correlation factors [16]. The correlation effects will reduce the conductivity at higher dopant fractions, resulting in a more pronounced maximum. The same applies to the percolation phenomena, e.g. of pathways only across A-A edges, that have been considered in detail in reference [15] but have been neglected in our investigation.

Finally we can draw the following conclusion. Our model for a strongly acceptor-doped, fluorite-type oxygen ion conductor, (e.g. A=Zr, B=Y) shows, despite of the approximations we have made and the resulting limitations, that the oxygen ion conductivity is not only determined by the jump rates through the A-A, A-B and B-B edges but to a similar extent by the vacancy distribution to the cation tetrahedra. The maximum in the conductivity and the increase in activation energy with the dopant fraction are due to vacancy binding in the B-containing cation tetrahedra combined with reduced jump rates across A-B and B-B edges.

3. Cation tracer diffusion in LSGM

In oxides with dominating oxygen disorder cation defects are only minority defects and consequently cation diffusion is much slower than oxygen diffusion. Cation diffusion is nevertheless important since the slowest moving species determine many fundamental processes, such as sintering [22], creep [23] or internal friction [24].

An important example is yttria stabilized zirconia, $(Zr_{1-x}Y_x)O_{2-x/2}$ (YSZ). Cation diffusion studies [25,26,27] show that Zr diffusion becomes slower with increasing Y-content. This is due to the fact that the dopant yttrium determines the fraction of oxygen vacancies, which again determines via the Schottky equilibrium ($\mathrm{nil} \leftrightarrow V_{Zr}''' + 2V_O^{\bullet\bullet}$) the fraction of cation vacancies. Thus cation diffusion should be slower the higher the dopant fraction, as observed. As expected, comparison of the self-diffusion coefficients of oxygen and cations in YSZ shows that D_O is about 5 orders of magnitude larger than D_{cation}.

Similar results were found for doped lanthanum gallate, $La_{1-x}Sr_xGa_{1-y}Mg_yO_{3-(x+y)/2}$ (LSGM), which has a higher oxygen ion conductivity than YSZ and is therefore a candidate for solid oxide fuel cells working at intermediate temperatures [28]. Here oxygen diffusion coefficients [29] and impurity diffusion coefficients of several cations [30,31] have been measured.

In this chapter we summarize some recent results for tracer self-diffusion of lanthanum, strontium and magnesium in $La_{0.9}Sr_{0.1}Ga_{0.9}Mg_{0.1}O_{2.9}$ (LSGM1010) [32]. The diffusion experiments were performed with stable, strongly enriched isotopes of La, Sr and Mg, and the diffusion profiles were measured with ToF-SIMS depth profiling. Typical penetration profiles for ^{138}La, ^{84}Sr and ^{25}Mg obtained by SIMS are shown in Fig. 5. In each profile one can distinguish two different parts. At small penetration depths (up to 100 nm) the profile has a steep slope and refers to bulk diffusion. At larger penetration depths the slope decreases, and the profile refers to a mixture of grain boundary and bulk diffusion after Fisher's model [33] of simultaneous bulk and grain boundary diffusion in polycrystalline materials. The bulk diffusion coefficients of ^{138}La, ^{84}Sr and ^{25}Mg were obtained by fitting the thin-film solution [32] to the bulk part of the experimental profiles and are shown in Fig. 6 as a function of the inverse temperature. The apparent activation energies, E_a, were calculated from the local slope of these curves, $E_a = -R\cdot(\mathrm{d}\ \ln D/\mathrm{d}(1/T))$. It was found that the apparent activation energies of the tracer diffusion coefficients of ^{138}La, ^{84}Sr and ^{25}Mg change from about 1.5 eV at 900°C to about 4.5 eV at 1400°C.

The grain boundary diffusion coefficients which can be obtained from the tails of the diffusion profiles [34,35] are about three to four orders of magnitude higher than the bulk diffusion coefficients.

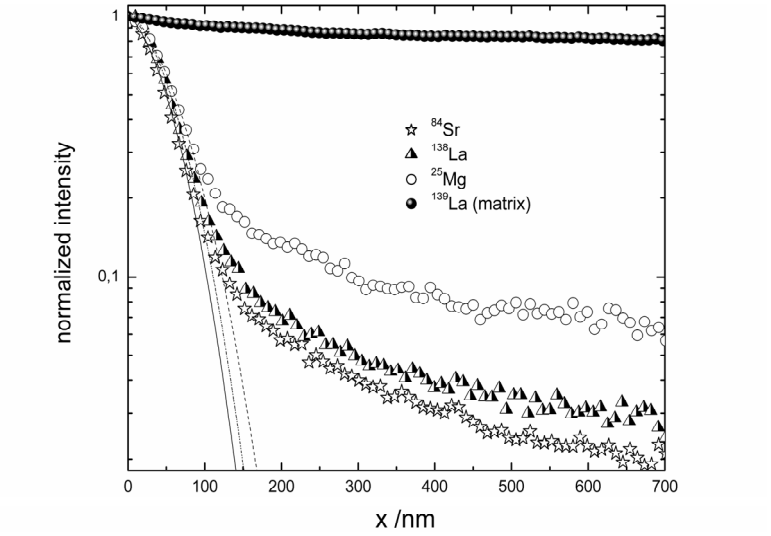

Fig. 5 Typical diffusion profiles of ^{138}La, ^{84}Sr and ^{25}Mg in polycrystalline $La_{0.9}Sr_{0.1}Ga_{0.9}Mg_{0.1}O_{2.9}$ measured by SIMS (T=1400°C, t_{diff}= 1.61 h). All profiles were corrected by the background signal of the corresponding isotope and the matrix-element ^{139}La and then normalized to 1. The lines show the fit of the thin film solution to the bulk part of the profiles [32].

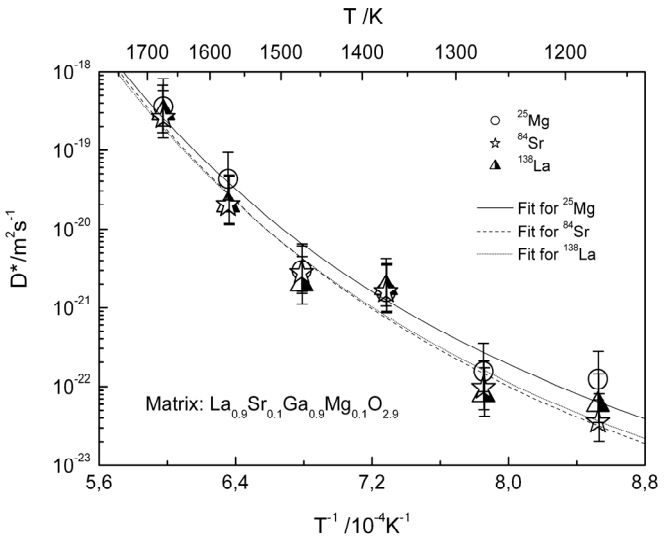

Fig. 6 Bulk diffusion coefficients of ^{138}La,^{84}Sr and ^{25}Mg in $La_{0.9}Sr_{0.1}Ga_{0.9}Mg_{0.1}O_{2.9}$ as a function of the inverse temperature.

In LSGM, acceptors, Sr'_{La} and Mg'_{Ga}, and charge compensating oxygen vacancies, $V_O^{\bullet\bullet}$ are the majority defects (see Introduction) while cation vacancies in the A- and B-sublattices of the perovskite LSGM are only minority defects. As a result, the cation diffusivities are very small, and at low temperatures it is nearly impossible to equilibrate LSGM samples (concerning their minority defect structure). This means, that the defect structure which was established at high temperatures will be frozen in at an intermediate temperature when the samples are cooled. Thus, the apparent activation energies of the diffusion coefficients should increase with increasing temperature, as observed experimentally. At low temperatures the values correspond to the migration energy of the cations (about 1.5-2 eV), whereas at high temperatures they correspond to the sum of the migration energy and the formation energy (2.5-3 eV) of the defects by which the cations are mobile.

The nearly identical cation migration energies and diffusion coefficients found in our experiments are in contradiction to the expectations for cation diffusion in a perovskite structure. Assuming a simple vacancy mechanism, diffusion of B cations should be much slower than diffusion of A cations, because B cations cannot perform direct nearest neighbor jumps, in contrast to A cations. Theoretical calculations of the cation migration energies support this expectation. Khan *et al.* [36] have obtained $E_{mig}(La_A) = 4.6$ eV and $E_{mig}(Ga_B) = 16.9$ eV, and De Souza and Maier [37] have calculated $E_{mig}(Sr_A) = 2.8$ eV, $E_{mig}(La_A) = 4.7$ eV and $E_{mig}(Ga_B) = 14.7$ eV. The large migration energy for B cations is caused by the fact that during that jump the B cation comes into close contact with the large A cation, which results in strong coulombic repulsion [37,38].

To explain our experimental observations we have proposed a more complicated diffusion mechanism [32]. Cation vacancies in the A- and B-sublattices, V_A''' and V_B''', and oxygen vacancies, $V_O^{\bullet\bullet}$, can form defect clusters which are strongly bound due to the coulombic forces between the defects. Already the most simple cluster, $\{V_A''', V_B''', V_O^{\bullet\bullet}\}$, enables a coupled transport of A- and B-cations. The cluster is shown in Fig. 7 in a two-dimensional projection of the cubic perovskite structure of LSGM. Note that oxygen ions and B-cations are in one plane while A-cations are located above (or below) that plane. The cluster can move through the lattice without dissociating into individual defects in four correlated steps. In the first step, an oxygen ion jumps to a vacant oxygen site, in step two an A-cation jumps to a vacant A-site, and in the third step another oxygen ion jumps into the oxygen vacancy. Now, in the fourth step, a B-cation can perform a jump to the nearest neighbor vacant B-site. This jump pathway is probably curved, but due to the adjacent, vacant A-site the B-cation does not come into close contact with the large A-cation. Thus, the corresponding activation energy should be much smaller than for the B-jumps considered in the atomistic simulations. As a result of the four correlated jumps, the whole cluster is displaced by half a lattice constant (as shown in the last part of Fig. 7), and both an A-cation and a B-cation have moved simultaneously. The activation energy of the whole process is determined by the step with the highest activation energy. Since the activation energy for a jump of an oxygen ion is only 0.6 eV [39] steps two or four must be rate determining (considering our experimental value of about 2 eV for the migration energy).

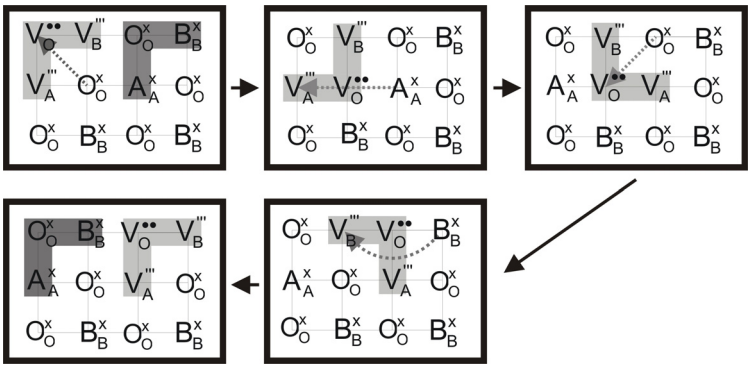

Fig. 7 Defect cluster, $\{V_A''', V_B''', V_O^{\bullet\bullet}\}$, in the perovskite LSGM and four-step jump mechanism by which the cluster is mobile without dissociation (two-dimensional projection of the cubic perovskite structure; oxygen ions and B-cations are in one plane while A-cations are located above or below that plane).

The implications of the postulated cluster mechanism in LSGM were considered recently [40] in a theoretical paper. Sum-rule expressions for the collective correlation factors were derived and found to be in excellent agreement with Monte Carlo calculations. Expressions were also developed for the tracer correlation factors of lanthanum and gallium for diffusion via the cluster mechanism and tested by Monte Carlo computer simulation. Good agreement was found. The calculations also show, that the ratio of the tracer diffusivities of A- and B-site cations, D_A/D_B, can only vary between 10^{-1} and 10^{1}, in good agreement with the experimental results (see Fig. 6).

3.1 Conclusions

Cation tracer diffusion coefficients of La, Sr and Mg have been measured in Sr- and Mg-doped lanthanum gallate, $La_{1-x}Sr_xGa_{1-y}Mg_yO_{3-(x+y)/2}$. The bulk diffusion coefficients are similar for all cations with apparent activation energies which are strongly dependent on temperature. To explain these findings the formation of a defect cluster was proposed which consists of vacancies in the A-, B- and O sublattices, $\{V_A''', V_B''', V_O^{\bullet\bullet}\}$. The cluster is strongly bound and can move through the perovskite lattice by a postulated four-jump diffusion mechanism without dissociation. In this way A- and B-cations are moved simultaneously resulting in identical diffusion coefficients. The observed increase of the apparent activation energy of the diffusion coefficients with increasing temperature is explained by a non-equilibrated defect structure of the minority defects at lower temperatures.

Acknowledgement
Financial support by Deutsche Forschungsgemeinschaft (DFG) and Fonds der Chemischen Industrie is gratefully acknowledged.

References

[1] H. Schmalzried, Solid State Reactions, VCH, Weinheim, 1981.
[2] A.R. Allnatt, A.B. Lidiard: Atomic Transport in Solids, Cambridge University Press, Cambridge, 1993.
[3] M. Martin, Diffusion in Oxides, In: Diffusion in Condensed Matter, Methods, Materials, Models, P. Heitjans, J. Kärger (Eds.) Springer (2005), pp 209-248.
[4] M. Schroeder, M. Martin, Thermodynamics of New Materials, in: Chemical thermodynamics for industry, T.M. Letscher (ed.), The Royal Society of Chemistry, Cambridge (2004) 180-196.
[5] A. Hammou, J. Guindet, in: The CRC Handbook of Solid State Electrochemistry, P.J. Gellings, H.J.M. Bouwmeester (Eds.), CRC Press, Boca Raton, 1996, p. 407.
[6] S.P.S. Badwal, Solid State Ionics 52 (1992) 23.
[7] P.S. Manning, J.D. Sirman, R.A. De Souza, J.A. Kilner, Solid State Ionics 100 (1997) 107.
[8] D.W. Stickler, W.G. Carlson, J. Am. Ceram. Soc. 47 (1964) 122.
[9] H. Inaba, H. Takawa, Solid State Ionics 83 (1996) 1.
[10] H. Schmalzried, Z. Phys. Chem. NF 105 (1977) 47.
[11] M.S. Khan, M.S. Islam, D.R. Bates, J. Mater. Chem. 8 (1998) 2229.
[12] M.O. Zacate, L. Minervini, D.J. Bradfield, R.W. Grimes, K.E. Sickafus, Solid State Ionics 128 (2000) 243.
[13] F. Shimojo, T. Okabe, F. Tachibana, M. Kobayashi, H. Okazaki, J. Phys. Soc. Japan, 61 (1992) 2842.
[14] F. Shimojo, H. Okazaki, J. Phys. Soc. Japan, 61 (1992) 4106.
[15] M. Meyer, N. Nicoloso, Ber. Bunsenges. Phys. Chem. 101 (1997) 1393.
[16] A.D. Murray, G.E. Murch, C.R.A. Catlow, Solid State Ionics 19 (1986) 196.
[17] R. Krishnamurthy, Y.-G. Yoon, D.J. Srolovitz, R. Carr, J. Am. Cer. Soc. 87 (2004) 1821.
[18] M. Martin, Z. Phys. Chem. 219 (2005) 105-122.
[19] M. Martin, J. Electroceram 17 (2006) 765-773.
[20] S.P.S. Badwal, F.T. Ciacchi, S. Rajendran, J. Drennan, Solid State Ionics 109 (1998) 167.
[21] R.E.W. Casselton, Phys. Status Solidi A 2 (1970) 571.
[22] Yet-Ming Chiang, Dunbar Bernie III, W. D. Kingery, Physical Ceramics, John Wiley & Sons, New York, 1977, chapter 5.
[23] J.L. Routbort, K.C. Goretta, R.E. Cook, J. Wolfenstine, Solid State Ionics 129 (2000) 53.
[24] M. Weller, Z. Metallk. 84 (1993) 381.
[25] H. Solmon, J. Chaumont, C. Dolin, C. Monty, Ceram. Trans. 24 (1991) 175.
[26] M. Kilo, G. Borchardt, S. Weber, S. Scherrer, K. Tinschert, Ber. Bunsenges. Phys. Chem. 101 (1997) 1361.
[27] M. Kilo, M.A. Taylor, Ch. Argirusis, G. Borchardt, B. Lesage, S. Weber, S. Scherrer, H.Scherrer, M. Schroeder, M. Martin, J. Appl. Phys. 94 (2003) 7547-7552.
[28] B.C.H. Steele: J. Materials Sci. 36 (2001) 1053.
[29] T. Ishihara, J.A. Kilner, M. Honda: Solid State Ionics 113-115 (1998) 593.

[30] O. Schulz, S. Flege, M. Martin,Solid Oxide Fuel Cells VIII (SOFC-VIII), S.C. Singhal M. Dokiya (Eds.), Proceedings of the Electrochemical Society, PV 2003-2007 (2003) pp. 304-314.
[31] A. Matraszek, D. Kobertz, L. Singheiser, K. Hilpert, W. Kuncewicz-Kupczyk, M. Miller, O. Schulz, M. Martin, Mat.-wiss. u. Werkstofftechn. 33 (2002) 355.
[32] O. Schulz, M. Martin, C. Argirusis, G. Borchardt, Phys. Chem. Chem. Phys. 5 (2003) 2308.
[33] J. C. Fisher, J. Appl. Phys. 22 (1951) 74.
[34] A. D. Le Claire, Brit. J. Appl. Phys. 14 (1963) 351.
[35] Y. C. Chung, B. J. Wuensch, Materials Letters 28 (1996) 47.
[36] M. S. Khan, M. S. Islam, D. R. Bates, J. Phys. Chem. 102 (1998) 3099.
[37] R. A. De Souza, J. Maier, Phys. Chem. Chem. Phys. 5 (2003) 740.
[38] R. A. De Souza, M. S. Islam, E. Ivers-Tiffée, J. Mater. Chem. 9 (1999) 1621.
[39] T. Ishihara, J. A. Kilner, M. Honda, Solid State Ionics 113-115 (1998) 593.
[40] I.V. Belova, G.E. Murch, D. Samuelis, M. Martin, Defect and Diffusion Forum 263 (2007) 81-86